Photocatalysis Hot Paper

International Edition: DOI: 10.1002/anie.201603331
German Edition: DOI: 10.1002/ange.201603331

An Elemental Phosphorus Photocatalyst with a Record High Hydrogen Evolution Efficiency

Zhuofeng Hu, Luyan Yuan, Zhifeng Liu, Zhurui Shen, and Jimmy C. Yu**

Abstract: *Semiconductive property of elementary substance is an interesting and attractive phenomenon. We obtain a breakthrough that fibrous phase red phosphorus, a recent discovered modification of red phosphorus by Ruck et al., can work as a semiconductor photocatalyst for visible-light-driven hydrogen (H_2) evolution. Small sized fibrous phosphorus is obtained by 1) loading it on photoinactive SiO_2 fibers or by 2) smashing it ultrasonically. They display the steady hydrogen evolution rates of 633 $\mu mol\,h^{-1}\,g^{-1}$ and 684 $\mu mol\,h^{-1}\,g^{-1}$, respectively. These values are much higher than previous amorphous P (0.6 $\mu mol\,h^{-1}\,g^{-1}$) and Hittorf P (1.6 $\mu mol\,h^{-1}\,g^{-1}$). Moreover, they are the highest records in the family of elemental photocatalysts to date. This discovery is helpful for further understanding the semiconductive property of elementary substance. It is also favorable for the development of elemental photocatalysts.*

Phosphorus (P) is one of the most widespread elements, and there is approximately 100 billion tons of phosphorus on the earth.[1] This element is of great significance in the field of chemistry, physics, biology and ecology etc.[1] Since its discovery in 1660s,[2] modifications of different kinds of P allotropes have received extensive attention.[3,4] Up to date, at least five kinds of P allotropes have been identified, including white, black, amorphous, violet (Hittorf) and fibrous P.[4h] Besides, many P allotropes have been theoretically predicted by Häser et al.[4c,d] in 2004, two of them have been successfully isolated from copper halide matrix by Pfitzner et al.[5]

White P is the most active one among the allotropes of P, and has been widely used in organic chemistry.[6] However, its high toxicity greatly limits its wider applications. By contrast, orthorhombic black P is considered to be thermodynamically stable.[7] It has a layered structure. The synthesis of black P often requires high pressure until Nilges et al. provide a method to easy access black P.[8] Very recently, the semiconducive property of exfoliated black P nanosheet is discovered,[7b,c] and has become one of the hottest topics in material science, for example as field effect transistor, photodetector, and sensor.[7b–g]

Compared with white and black allotropes, red P is more commonly used, inexpensive, and low-toxic. These advantages render red P a promising candidate in material physics and chemistry.[2,9] According to literatures, the amorphous and crystalline modifications of red P are based on tubular units of five- and six-membered rings.[3,4f,5] In the early literatures, the various red modifications were named as I-V types as their structures were not fully known.[4a] Among them, the structure of type V violet Hittorf P (monoclinic) was characterized in 1969 by Thurn and Krebs.[10] In the past decade, Pfitzner et al.[5] and Ruck et al.[4f] have prepared further tubular P allotropes. In 2005, fibrous P crystals (triclinic) are obtained via a CVD method from amorphous red P by Ruck et al.[4f] It is composed of the same tubes that existing in Hittorf P but arranged as parallel sets of covalently linked rods instead of layers of orthogonally linked rods.[3,11] This modification is then recognized as type IV of red modifications based on XRD patterns. Pfitzner et al. have prepared two novel solid red-brown P allotropes nanorods[5] from the adducts $(CuI)_8P_{12}$[12] and $(CuI)_3P_{12}$.[13] Another kind of P nanorod is found in $(CuI)_2P_{14}$.[14]

Although great progress has been achieved in preparation of red P modifications, the applications of the red P is still limited. In the past centuries, the red P was mainly used to prepare igniters, gunpowder and flame retardant.[2] Unlike highly active white P, it can only be used as P source in chemical reactions under some special condition like high-pressure UV light irradiation[15] or ionic liquid activation.[16] Recently, in the field of rechargeable battery, red P has shown high capacitance via reversible reactions with lithium ions or sodium ions.[17] Also, unlike black P, the semiconductive property and related application of red P (amorphous, Hittorf, and fibrous) is rarely reported. Recently, our group has preliminarily discussed the probability of using red P as a semiconductor for photocatalytic water splitting. But the low activity of previously-reported amorphous and Hittorf red P greatly restrict the practical applications of red P.

In our viewpoint, the potential of red P as a semiconductor has not been fully realized. First, according to the general rule of "structure-property" relationship, it is quite meaningful and attractive to further study other red P modifications as the semiconductive photocatalyst. Second, prior reports mainly focused on amorphous, large-grain and poor-distributed red P particles, which tend to cause serious charge

[*] Dr. Z. H. Hu, L. Y. Yuan, Prof. Z. F. Liu, Dr. Z. R. Shen, Prof. J. C. Yu
Department of Chemistry
The Chinese University of Hong Kong, Shatin
New Territories, Hong Kong (China)
E-mail: jimyu@cuhk.edu.hk
Dr. Z. R. Shen
Key Laboratory of Advanced Ceramics and
Machining Technology, Ministry of Education
School of Materials Science and Engineering
Tianjin University, Tianjin 300072 (China)
E-mail: shenzhurui@tju.edu.cn
Dr. Z. H. Hu, Dr. Z. R. Shen, Prof. J. C. Yu
Shenzhen research institute
The Chinese University of Hong Kong
Shenzhen (China)

Supporting information for this article can be found under: http://dx.doi.org/10.1002/anie.201603331.

recombination. Therefore, it is highly desirable to prepare a small-sized and uniformly distributed product.

Herein, we for the first time use fibrous phase red P, a recent discovered modification by Ruck et al.,[4f] as a semiconductor for photocatalytic hydrogen evolution. Small sized fibrous P is obtained by two methods: 1) We uniformly distributed submicron-sized fibrous red P on photoinactive SiO_2 fibers via a CVD process (Scheme 1 left part, donated as

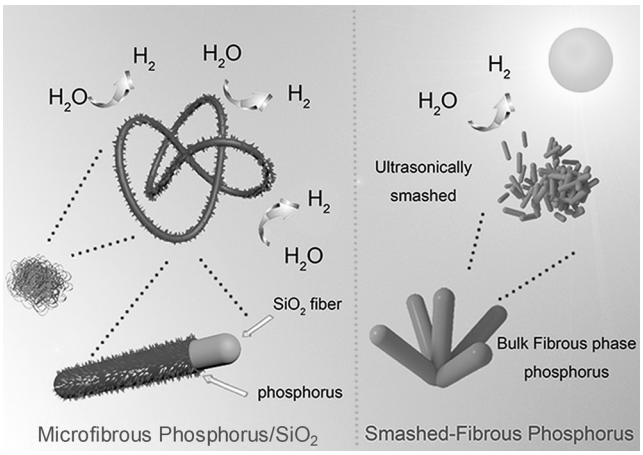

Scheme 1. The diagram of photoactive micro-fibrous P/SiO_2 (left) and smashed-fibrous P based on fibrous phase red P (Right).

"micro-fibrous P/SiO_2"). 2) Also, we prepared bulk single-phase fibrous P according to literature,[4g] and smashed them into microstructures (Scheme 1 right part, donated as "smashed-fibrous P"). The estimated activity of phosphorus in the micro-fibrous P/SiO_2 in photocatalytic hydrogen evolution reaches 633 $\mu mol\,h^{-1}\,g^{-1}$. While the activity of smashed-fibrous P reaches 684 $\mu mol\,h^{-1}\,g^{-1}$. These values increase by about 1055/1138 and 396/427 times compared to those previous reported bulk amorphous and Hittorf P, respectively.[18] Moreover, these values are the highest records in the family of elemental photocatalysts including silicon (Si),[19] boron (B),[20] carbon (C),[21] sulfur (S)[22] and selenium (Se)[23] (a recent record of steady hydrogen evolution rate is about 400 $\mu mol\,h^{-1}\,g^{-1}$ for mesoporous elemental Si under full-spectrum illumination)[19] Besides, the red P is more stable than Si in water under irradiation, because Si will be deactivated by the surface oxidation reaction.

Micro-fibrous P/SiO_2 is prepared from amorphous red P and SiO_2 fibers wool via a CVD method (see Scheme S1 of the Experimental Section in the Supporting Information). SiO_2 is chosen as a support, because it is photoinactive (Section S1, Figure S1) that the activity in photocatalytic hydrogen evolution can be ascribed to the red P. Also, it is highly-dispersed and thermally stable, which is helpful for the distribution and deposition of red P.

Compared with bare SiO_2 fibers (Figure S2a), some one-dimensional (1D) microstructures can be seen on the surface of the micro-fibrous P/SiO_2 (Figure S2b). The corresponding EDX spectrum shows strong signals of P, Si and O (Figure S3, Table S1), which is consistent with its chemical composition. Some short submicron rods with the size of c.a. 500 nm ~ 1 μm can be observed in the enlarged SEM image (Figure 1a). Its HRTEM image shows a crystal facet with the *d*-spacing of 5.81 Å, which is the characteristic of (001) facets of fibrous-phase red P (Figure S2c).[4f]

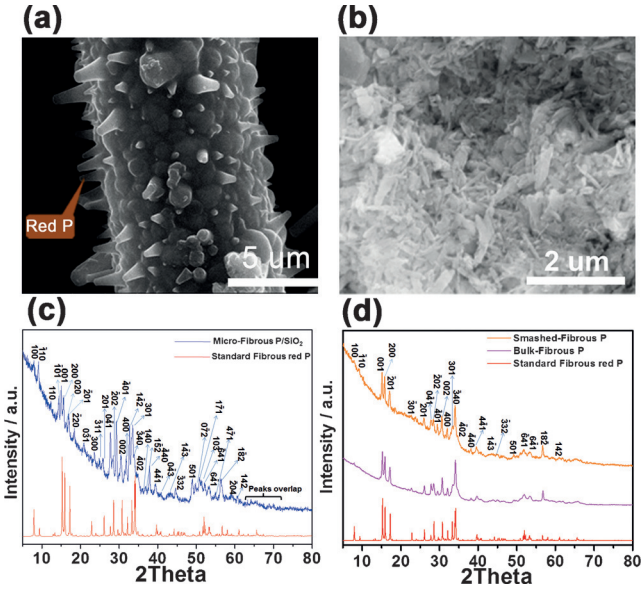

Figure 1. SEM images of a) micro-fibrous P/SiO_2, b) smashed-fibrous P, and XRD patterns of c) micro-fibrous P/SiO_2 and d) smashed-fibrous P, bulk-fibrous P. The standard XRD patterns of fibrous red P are placed in (c) and (d) as the references.

For smashed-fibrous P, the single phase bulk fibrous P is prepared according to literature,[4g] and are smashed into submicron particles (see experimental section). As shown in Figure 1b, its size is as small as 300 nm–1 μm.

To study the chemical structure of these two samples, XRD, Raman and FT-IR analysis are performed (Figure 1c,d, Section S2, Table S2, Figure S4-Figure S10). The XRD patterns of micro-fibrous P/SiO_2 and smashed-fibrous P (Figure 1c,d, Table S2) are well indexed into the simulated pattern of triclinic fibrous-phase red P (CSD. 391323).[4f] However, the pattern of micro-fibrous P/ SiO_2 shows the relative low crystallinity (Figure 1c, Table S2). It is known that some P allotropes have similar crystalline characteristic with fibrous P, for example, the Hittrof P, [P8]P4(4)[, [P10]P2[, and [P12(4)]P2[. Comparison of their XRD patterns shows that 1) phosphorus in micro-fibrous P/SiO_2 should be mainly composed of fibrous P; 2) it cannot fully exclude the presence of other P allotropes, especially [P10]P2[and [P12(4)]P2[(details see Section S2, Table S2, Figure S4–Figure S8). As shown in Figure S9, the Raman spectra of the two samples resemble to each other. They both exhibit the peaks of fibrous-phase P, and are quite different from those of other phosphorus allotropes[24] and SiO_2. This result is consistent with the XRD analysis, and further confirms their chemical structures of fibrous P.

The band structure of fibrous P is important for understanding its photocatalytic activity. It is known that the fibrous P is composed of [P_{21}] polyphosphide tubes as the basic

building units, and it has a layered structure. The electronic structure of fibrous P was first investigated by Ruck et al.[4f] On the base of his crystal structure, we carry out the theoretical calculation to study the band structure of fibrous P. Van der Waals correction (Grimme d2) is introduced in the calculations.[25] (Figure 2a,b). The calculated band structure

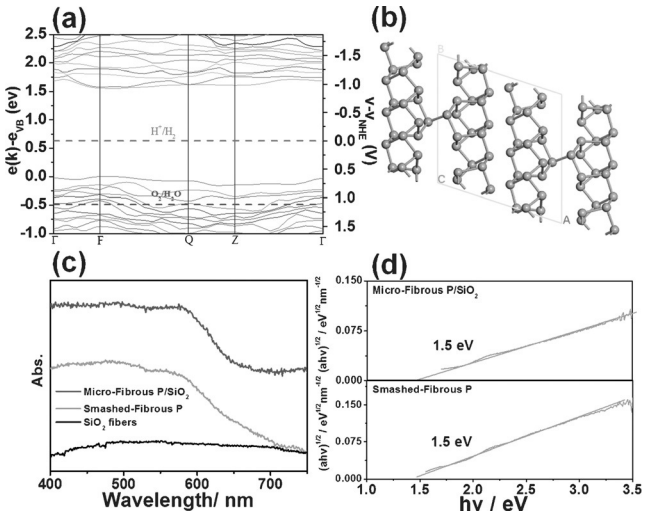

Figure 2. a) Theoretical calculation of the band structure of fibrous P. b) Atomic structure of fibrous P simulated in the theoretical calculation. c) Absorption spectrum of the micro-fibrous P/SiO_2, smashed-fibrous P and SiO_2 fibers. d) Kubelka–Munk plots converted from the absorption spectrum of micro-fibrous P/SiO_2 (up) and smashed-fibrous P (down).

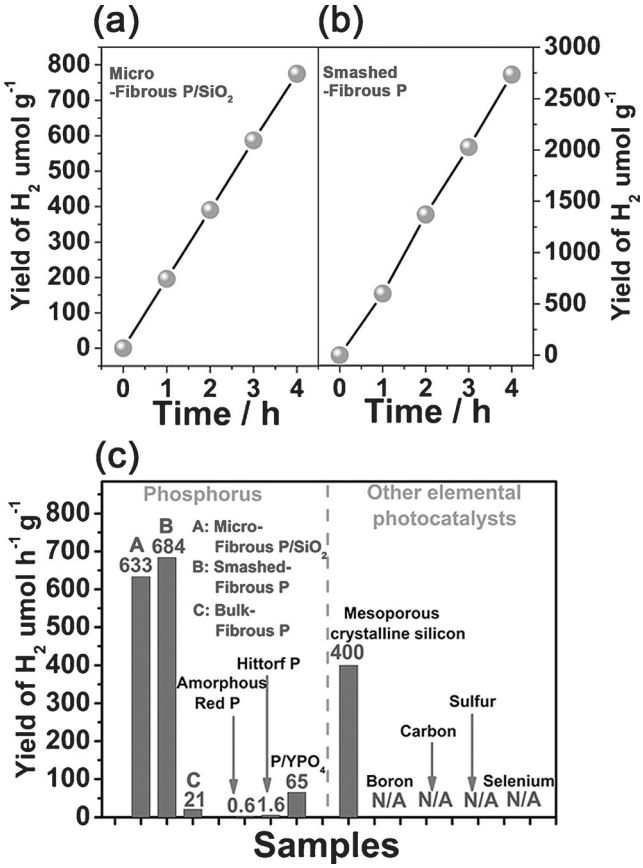

Figure 3. Time course of the hydrogen evolution on a) micro-fibrous P/SiO_2 and b) smashed-fibrous P. c) Comparison of activity of photocatalytic hydrogen evolution on different elemental photocatalysts.[18–23] The light source used or referred here are all visible light, except the mesoporous crystalline Si (full spectrum).

of slab exposing (0 $\bar{1}$ 0) surface are shown in Figure 2a.The fibrous P clearly exhibits a band gap of 1.5 eV according to the projector-augmented-wave method with Perdew-Burke-Ernzerhof GGA functional. It is the typical characteristic of a semiconductor. This value is in well agreement with the absorption spectra of micro-fibrous P/SiO_2 and smashed-fibrous P (Figure 2c,d). This result also indicates that the fibrous P is a direct band gap semiconductor. Thus, it compares favorably with Si (indirect band gap) that has energy loss during excitation. Importantly, it has a very high conduction band minimum of −0.9 V vs. NHE. This is higher than the theoretical potential of hydrogen evolution (0 V vs. NHE). Also, this is much higher than previously reported Hittorf red P (−0.25 eV) and Si (−0.2–−0.35 eV),[18b,26] indicating the fibrous P is more energetically favorable for water reduction.[19,27] The larger energy gap between the conduction band edge and the H^+/H_2 potential for fibrous red P is remarkably beneficial for water reduction, which should be one of the reason for higher photocatalytic activity of fibrous-phase red P (Figure 3).

The yield of hydrogen from photocatalytic water splitting was evaluated by using methanol as a sacrificial reagent and Pt as a cocatalyst. Hydrogen generation over time was evacuated at interval of 1 h under visible light irradiation ($\lambda > 420$ nm). The yield of hydrogen for micro-fibrous P/SiO_2 is about 196 $\mu mol\,h^{-1}\,g^{-1}$ (Figure 3a). Moreover, in the recycling experiment, its hydrogen yield is very steady (Figure S11). Regarding that the fibrous P accounts for 31 wt% in the composite (EDX results, Table S1) and that the SiO_2 fiber is photoinactive (Section S1, Figure S1), the activity of fibrous P in mcirofibrous P/SiO_2 is estimated to be 633 $\mu mol\,h^{-1}\,g^{-1}$. A similar value of 684 $\mu mol\,h^{-1}\,g^{-1}$ is obtained for the smashed-fibrous P (Figure 3b). These are the highest values among elemental photocatalysts for visible-light-driven hydrogen evolution from water (Figure 3c, right part). These are almost 1.5 times as high as that of the mesoporous crystalline Si (full spectrum),[19] while other elemental photocatayst are rarely reported to be able to produce hydrogen photocatalytically.[20–23] These are also much higher than previous reported elemental P including amorphous red P,[18b] Hittorf P,[18b] and amorphous P/YPO_4 (Figure 3c, left part).[18a] Besides, these values are about a quarter of the activity of TiO_2 (P25, 2500 $\mu mol\,h^{-1}\,g^{-1}$, full-spectrum illumination) and CdS (2200 $\mu mol\,h^{-1}\,g^{-1}$, visible light illumination) when using the same testing instrument. In the control experiments in the dark, no obvious hydrogen generation are observed for both of micro-fibrous P/SiO_2 and smashed-fibrous P, indicating the chemical stability of fibrous P in water. It is also reported that only trace levels of phosphate (PO_4^{3-}) and hydrogen phosphate (HPO_4^{2-}) ions are detected after long-term photocatalytic reaction of red

P.[18b,28] Moreover, the P 2p fine XPS spectra also indicate that the chemical states of fibrous P is stable after the photocatalytic reaction (Figure S12 and the explanation). This further confirms the chemical stability of fibrous P in photocatalysis.

The reason for the high activity of micro-fibrous P/SiO_2 and smashed-fibrous P is then discussed here. First, as mentioned before, high conduction band minimum (−0.9 eV vs. NHE) of fibrous-phase P contributes to their superior activity. Moreover, the microstructure of fibrous P in micro-fibrous P/SiO_2 and smashed-fibrous P are extensively in contact with water, achieving a high activity of photocatalytic hydrogen evolution. The microstructure is very helpful to obtain higher charge transfer efficiency. To study in detail, micro-fibrous P/SiO_2 is chosen as the example and compared with bulk fibrous P (denoted as "bulk-fibrous P"). They were fabricated into electrodes by depositing them on bare FTO conducting glasses. Both of them can produce repeatable cathodic photocurrent upon visible illumination at 0.2 V vs. RHE (Figure 4a,b), indicating the generation of photoexcited charge carriers and the semiconductor nature of fibrous P. This also confirms the p-type property of fibrous P,[29] which is consistent with the previous report.[18b]

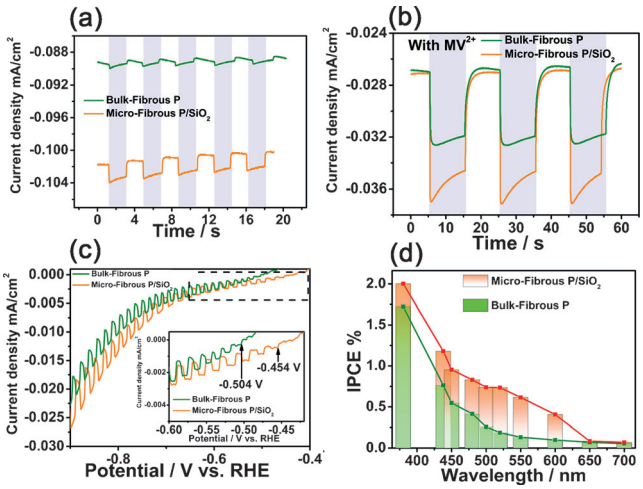

Figure 4. Photocurrent density of micro-fibrous P/SiO_2 and a control sample of bulk-fibrous P under simulated sunlight in 0.1 M Na_2SO_4 electrolyte a) with and b) without 0.001 M methylviologen dichloride ($MVCl_2$). c) Voltammograms of micro-fibrous P/SiO_2 and bulk-fibrous P under chopped simulated sunlight in 0.1 M Na_2SO_4 electrolyte with 0.001 M $MVCl_2$. d) IPCE curve of micro-fibrous P/SiO_2 and bulk-fibrous P.

The surface charge transfer efficiency η_{trans} is measured by adding a fast electrons scavenger methylviologen dichloride ($MVCl_2$) to the electrolyte.[30] According to literature, the photocurrent can be expressed as Equation (1),[30]

$$J_{H_2O} = J_{max}\eta_{abs}\eta_{sep}\eta_{trans} \quad (1)$$

where J_{H_2O} and J_{max} is the measured and the theoretical maximum photocurrent in the absence of electrons scavenger, respectively; η_{abs} is the light absorption efficiency; η_{sep} is the charge separation efficiency inside the photoanode; and η_{trans} surface charge transfer efficiency of the photoanode.

In the presence of electron scavenger MV^{2+}, the surface charge transfer is very fast and $\eta_{trans} \approx 100\,\%$. The photocurrent can be expressed as Equation (2).

$$J_{MV^{2+}} = J_{max}\eta_{abs}\eta_{sep} \quad (2)$$

Since the addition of MV^{2+} did not change the light absorption, pH and η_{sep}. J_{max}, η_{abs} and η_{sep} are unaltered for both J_{H_2O} and $J_{MV^{2+}}$. Therefore, the surface transfer efficiency can be calculated by comparing the photocurrent from water and MV^{2+} reduction [Eq. (3)].[30]

$$\eta_{trans} = J_{H_2O}/J_{MV^{2+}} \quad (3)$$

With the addition of MV^{2+}, the photocurrent density of bulk-fibrous P increases from 0.35 μA cm^{-2} to 5.5 μA cm^{-2}, while that of micro-fibrous P/SiO_2 increases from 2.4 μA cm^{-2} to 9.9 μA cm^{-2}. This increment is ascribed to easier reduction of MV^{2+} than water molecules. The η_{trans} of bulk-fibrous P is calculated to be 6.36 % and η_{trans} of micro-fibrous P/SiO_2 increases by a factor of 3.8 to 24.2 %. This suggests the submicron sized fibrous P in micro-fibrous P/SiO_2 shows much faster charge transfer efficiency than its bulk counterpart. This should be due to the smaller particle size and shorter carrier diffusion distance, which enables faster electron injection into the redox couple in the liquid phase.

In addition, we further investigate the density of charge carriers, an important parameter to evaluate a photocatalyst. In the presence of fast electron acceptor, it is reported that the photocurrent onset potential in a voltammograms reflects the quasi Fermi level of majority carriers.[31] Since there is hardly any overpotential for the reduction of fast electron acceptor MV^{2+}, charge carrier can migrate to the external circuit for photocurrent generation once the applied bias reaches the quasi Fermi level.[31] As shown in the insert in Figure 4c, the potential of micro-fibrous P/SiO_2 (−0.454 V vs. RHE) is 0.05 V positive than the bulk-fibrous P (0.504 V vs. RHE). In the quasi Fermi level, the carrier density difference between micro-fibrous P/SiO_2 and its bulk counterpart can be calculated according to the Nernst equation [Eq. (4)],[32]

$$E_{f1} - E_{f2} = kT\ln(N_{f1}/N_{f2})/e \quad (4)$$

where E_{f1} and N_{f1} is the quasi Fermi level and the carrier density at the Fermi level of sample 1, E_{f2} and N_{f2} is the corresponding values of sample 2, k the Boltzmann's Constant, T the temperature and e the the elementary charge.

Then, the 0.05 V shift corresponds to 7.0 times higher carrier density in the micro-fibrous P/SiO_2, which is greatly beneficial to photocatalytic water splitting.

The incident photon-to-current efficiency (IPCE) measurements were carried out according to the following Equation (5),[33]

$$IPCE = (1240 \times I)/(\lambda \times J_{light}) \quad (5)$$

where I is the photocurrent density (mA cm^{-2}), λ the incident light wavelength (nm), and J_{light} the power density of monochromatic light at a specific wavelength (mW cm^{-2}).

Results show that the micro-fibrous P/SiO_2 exhibits a higher IPCE than the bulk-fibrous P between 360–650 nm (Figure 4d). Besides, they show identical low-energy threshold of 650 nm, confirming the unaltered light absorption and band gap of the micro-fibrous P/SiO_2. Therefore, in the visible-light-driven hydrogen evolution, the submicron sized fibrous P in micro-fibrous P/SiO_2 displays c.a. 30 times activity than that of bulk-fibrous P (21 μmol $g^{-1}h^{-1}$, Figure 3c left part).

In summary, an elemental photocatalyst of fibrous phase red phosphorus has been developed here. The phosphorus in micro-fibrous P exhibits the record high visible-light-driven hydrogen evolution rates of 633 μmol. $h^{-1}g^{-1}$. Despite the small uncertainty in phase composition, the sample is beneficial to practical application due to its convenient preparation and easy recycling. The smashed-fibrous P exhibits the hydrogen evolution rates of 684 μmol. $h^{-1}g^{-1}$. These values are much higher than previous amorphous P (0.6 μmol $h^{-1}g^{-1}$) and Hittorf P (1.6 μmol $h^{-1}g^{-1}$). Moreover, these values are the highest ones among the elemental photocatalysts. The semiconductor property of the fibrous red P is confirmed by theoretical calculation and photocurrent generation. The high activity is ascribed to higher charge transfer efficiency and higher carrier density of the fibrous P microstructures. This discovery is helpful for further understanding the semiconductive property of red P. It is also favorable for the development of elemental photocatalysts.

Acknowledgements

This work was partially supported by the Shenzhen Basic Research Scheme (JCYJ20120619151417947) and grants from the Research Grants Council of the Hong Kong Special Administrative Region, China, under Theme-based Research Scheme through project numbers T23-407/13-N and 14304315. This work was also supported by the National Natural Science Foundation of China (grant numbers 21173179 and 21303118).

Keywords: photocatalysis · hydrogen evolution · phosphorus · semiconductors · sustainable chemistry

How to cite: *Angew. Chem. Int. Ed.* **2016**, *55*, 9580–9585
Angew. Chem. **2016**, *128*, 9732–9737

[1] a) Y. Fujita, H. O. Venterink, P. M. van Bodegom, J. C. Douma, G. W. Heil, N. Holzel, E. Jablonska, W. Kotowski, T. Okruszko, P. Pawlikowski, P. C. de Ruiter, M. J. Wassen, *Nature* **2014**, *505*, 82–86; b) B. C. Koo, Y. H. Lee, D. S. Moon, S. C. Yoon, J. C. Raymond, *Science* **2013**, *342*, 1346–1348; c) T. Low, R. Roldan, H. Wang, F. N. Xia, P. Avouris, L. M. Moreno, F. Guinea, *Phys. Rev. Lett.* **2014**, *113*, 5; d) A. Velian, C. C. Cummins, *Science* **2015**, *348*, 1001–1004.

[2] M. Scheer, G. Balázs, A. Seitz, *Chem. Rev.* **2010**, *110*, 4236–4256.

[3] F. Bachhuber, J. von Appen, R. Dronskowski, P. Schmidt, T. Nilges, A. Pfitzner, R. Weihrich, *Angew. Chem. Int. Ed.* **2014**, *53*, 11629–11633; *Angew. Chem.* **2014**, *126*, 11813–11817.

[4] a) W. L. Roth, T. W. DeWitt, A. J. Smith, *J. Am. Chem. Soc.* **1947**, *69*, 2881–2885; b) M. E. Barr, B. R. Adams, R. R. Weller, L. F. Dahl, *J. Am. Chem. Soc.* **1991**, *113*, 3052–3060; c) M. Haeser, *J. Am. Chem. Soc.* **1994**, *116*, 6925–6926; d) H. Hartl, *Angew. Chem. Int. Ed. Engl.* **1996**, *34*, 2637–2638; *Angew. Chem.* **1995**, *107*, 2857–2859; e) J. Legros, C. Bolm, *Angew. Chem. Int. Ed.* **2004**, *43*, 4225–4228; *Angew. Chem.* **2004**, *116*, 4321–4324; f) M. Ruck, D. Hoppe, B. Wahl, P. Simon, Y. Wang, G. Seifert, *Angew. Chem. Int. Ed.* **2005**, *44*, 7616–7619; *Angew. Chem.* **2005**, *117*, 7788–7792; g) N. Eckstein, A. Hohmann, R. Weihrich, T. Nilges, P. Schmidt, *Z. Anorg. Allg. Chem.* **2013**, *639*, 2741–2743; h) S. Lange, M. Bawohl, R. Weihrich, T. Nilges, *Angew. Chem. Int. Ed.* **2008**, *47*, 5654–5657; *Angew. Chem.* **2008**, *120*, 5736–5739.

[5] A. Pfitzner, M. F. Bräu, J. Zweck, G. Brunklaus, H. Eckert, *Angew. Chem. Int. Ed.* **2004**, *43*, 4228–4231; *Angew. Chem.* **2004**, *116*, 4324–4327.

[6] a) M. Arrowsmith, M. S. Hill, A. L. Johnson, G. Kociok-Kohn, M. F. Mahon, *Angew. Chem. Int. Ed.* **2015**, *54*, 7882–7885; *Angew. Chem.* **2015**, *127*, 7993–7996; b) P. Mal, B. Breiner, K. Rissanen, J. R. Nitschke, *Science* **2009**, *324*, 1697–1699.

[7] a) C. M. Park, H. J. Sohn, *Adv. Mater.* **2007**, *19*, 2465; b) H. Liu, A. T. Neal, Z. Zhu, Z. Luo, X. F. Xu, D. Tomanek, P. D. D. Ye, *ACS Nano* **2014**, *8*, 4033–4041; c) L. Li, Y. Yu, G. J. Ye, Q. Ge, X. Ou, H. Wu, D. Feng, X. H. Chen, Y. Zhang, *Nat. Nanotechnol.* **2014**, *9*, 372–377; d) H. Yuan, X. Liu, F. Afshinmanesh, W. Li, G. Xu, J. Sun, B. Lian, A. G. Curto, G. Ye, Y. Hikita, Z. Shen, S.-C. Zhang, X. Chen, M. Brongersma, H. Y. Hwang, Y. Cui, *Nat. Nanotechnol.* **2015**, *10*, 707–713; e) J. Kim, S. S. Baik, S. H. Ryu, Y. Sohn, S. Park, B. G. Park, J. Denlinger, Y. Yi, H. J. Choi, K. S. Kim, *Science* **2015**, *349*, 723–726; f) L. Viti, J. Hu, D. Coquillat, W. Knap, A. Tredicucci, A. Politano, M. S. Vitiello, *Adv. Mater.* **2015**, *27*, 5567–5572; g) A. Favron, E. Gaufres, F. Fossard, A. L. Phaneuf-L'Heureux, N. Y. W. Tang, P. L. Levesque, A. Loiseau, R. Leonelli, S. Francoeur, R. Martel, *Nat. Mater.* **2015**, *14*, 826.

[8] a) S. Lange, P. Schmidt, T. Nilges, *Inorg. Chem.* **2007**, *46*, 4028–4035; b) B. Liu, M. Köpf, A. N. Abbas, X. Wang, Q. Guo, Y. Jia, F. Xia, R. Weihrich, F. Bachhuber, F. Pielnhofer, H. Wang, R. Dhall, S. B. Cronin, M. Ge, X. Fang, T. Nilges, C. Zhou, *Adv. Mater.* **2015**, *27*, 4423–4429; c) T. Nilges, M. Kersting, T. Pfeifer, *J. Solid State Chem.* **2008**, *181*, 1707–1711.

[9] a) J. A. Young, *J. Chem. Educ.* **2004**, *81*, 945; b) E. C. Koch, *Propellants Explos. Pyrotech.* **2008**, *33*, 165–176; c) K. Sládková, J. Houska, J. Havel, *Rapid Commun. Mass Spectrom.* **2009**, *23*, 3114–3118.

[10] H. Thurn, H. Krebs, *Acta Crystallogr. Sect. B* **1969**, *25*, 125–135.

[11] A. Pfitzner, *Angew. Chem. Int. Ed.* **2006**, *45*, 699–700; *Angew. Chem.* **2006**, *118*, 714–715.

[12] M. H. Möller, W. Jeitschko, *J. Solid State Chem.* **1986**, *65*, 178–189.

[13] A. Pfitzner, E. Freudenthaler, *Angew. Chem. Int. Ed. Engl.* **1995**, *34*, 1647–1649; *Angew. Chem.* **1995**, *107*, 1784–1786.

[14] A. Pfitzner, S. Zimmerer, *Angew. Chem. Int. Ed. Engl.* **1997**, *36*, 982–984; *Angew. Chem.* **1997**, *109*, 1031–1033.

[15] M. Ceppatelli, R. Bini, M. Caporali, M. Peruzzini, *Angew. Chem. Int. Ed.* **2013**, *52*, 2313–2317; *Angew. Chem.* **2013**, *125*, 2369–2373.

[16] M. F. Groh, S. Paasch, A. Weiz, M. Ruck, E. Brunner, *Eur. J. Inorg. Chem.* **2015**, 3991–3994.

[17] a) Y. Kim, Y. Park, A. Choi, N.-S. Choi, J. Kim, J. Lee, J. H. Ryu, S. M. Oh, K. T. Lee, *Adv. Mater.* **2013**, *25*, 3045–3049; b) Y. Zhu, Y. Wen, X. Fan, T. Gao, F. Han, C. Luo, S.-C. Liou, C. Wang, *ACS Nano* **2015**, *9*, 3254–3264.

[18] a) F. Wang, C. Li, Y. Li, J. C. Yu, *Appl. Catal. B* **2012**, *119–120*, 267–272; b) F. Wang, W. K. H. Ng, J. C. Yu, H. Zhu, C. Li, L. Zhang, Z. Liu, Q. Li, *Appl. Catal. B* **2012**, *111–112*, 409–414.

[19] F. Dai, J. Zai, R. Yi, M. L. Gordin, H. Sohn, S. Chen, D. Wang, *Nat. Commun.* **2014**, *5*, 3605.

[20] G. Liu, L.-C. Yin, P. Niu, W. Jiao, H.-M. Cheng, *Angew. Chem. Int. Ed.* **2013**, *52*, 6242 – 6245; *Angew. Chem.* **2013**, *125*, 6362 – 6365.
[21] M. Xing, W. Fang, X. Yang, B. Tian, J. Zhang, *Chem. Commun.* **2014**, *50*, 6637 – 6640.
[22] G. Liu, P. Niu, L. Yin, H.-M. Cheng, *J. Am. Chem. Soc.* **2012**, *134*, 9070 – 9073.
[23] Y.-D. Chiou, Y.-J. Hsu, *Appl. Catal. B* **2011**, *105*, 211 – 219.
[24] R. A. L. Winchester, M. Whitby, M. S. P. Shaffer, *Angew. Chem. Int. Ed.* **2009**, *48*, 3616 – 3621; *Angew. Chem.* **2009**, *121*, 3670 – 3675.
[25] F. Bachhuber, J. von Appen, R. Dronskowski, P. Schmidt, T. Nilges, A. Pfitzner, R. Weihrich, *Z. Kristallogr.-Cryst. Mater.* **2015**, *230*, 107 – 115.
[26] P. D. Tran, V. Artero, M. Fontecave, *Energy Environ. Sci.* **2010**, *3*, 727 – 747.
[27] G. Liu, P. Niu, H.-M. Cheng, *ChemPhysChem* **2013**, *14*, 885 – 892.
[28] D. Xia, Z. Shen, G. Huang, W. Wang, J. C. Yu, P. K. Wong, *Environ. Sci. Technol.* **2015**, *49*, 6264 – 6273.
[29] a) J. N. Nian, C. C. Tsai, P. C. Lin, H. S. Teng, *J. Electrochem. Soc.* **2009**, *156*, H567 – H573; b) L. B. Xiong, S. Huang, X. Yang, M. Q. Qiu, Z. H. Chen, Y. Yu, *Electrochim. Acta* **2011**, *56*, 2735 – 2739.
[30] a) P. M. Rao, L. Cai, C. Liu, I. S. Cho, C. H. Lee, J. M. Weisse, P. Yang, X. Zheng, *Nano Lett.* **2014**, *14*, 1099 – 1105; b) G. Liu, J. Shi, F. Zhang, Z. Chen, J. Han, C. Ding, S. Chen, Z. Wang, H. Han, C. Li, *Angew. Chem. Int. Ed.* **2014**, *53*, 7295 – 7299; *Angew. Chem.* **2014**, *126*, 7423 – 7427.
[31] a) J. Zhao, M. A. Holmes, F. E. Osterloh, *ACS Nano* **2013**, *7*, 4316 – 4325; b) R. L. Chamousis, F. E. Osterloh, *Energy Environ. Sci.* **2014**, *7*, 736 – 743.
[32] a) B. A. Nail, J. M. Fields, J. Zhao, J. Wang, M. J. Greaney, R. L. Brutchey, F. E. Osterloh, *ACS Nano* **2015**, *9*, 5135 – 5142; b) I. A. Digdaya, L. Han, T. W. F. Buijs, M. Zeman, B. Dam, A. H. M. Smets, W. A. Smith, *Energy Environ. Sci.* **2015**, *8*, 1585 – 1593; c) J. C. Hill, A. T. Landers, J. A. Switzer, *Nat. Mater.* **2015**, *14*, 1150 – 1155.
[33] a) Y. Ling, G. Wang, D. A. Wheeler, J. Z. Zhang, Y. Li, *Nano Lett.* **2011**, *11*, 2119 – 2125; b) S. Hoang, S. W. Guo, N. T. Hahn, A. J. Bard, C. B. Mullins, *Nano Lett.* **2012**, *12*, 26 – 32; c) M. Xu, P. Da, H. Wu, D. Zhao, G. Zheng, *Nano Lett.* **2012**, *12*, 1503 – 1508; d) J. Su, X. Feng, J. D. Sloppy, L. Guo, C. A. Grimes, *Nano Lett.* **2011**, *11*, 203 – 208; e) J. Zhang, J. H. Bang, C. Tang, P. V. Kamat, *ACS Nano* **2010**, *4*, 387 – 395.

Received: April 5, 2016
Published online: May 4, 2016

